Hamiltonian Hopping for Efficient Chiral Mode Switching in Encircling Exceptional Points

Aodong Li,[1,*] Jianji Dong,[1,*] Jian Wang,[1,*] Ziwei Cheng,[1] John S. Ho,[2] Dawei Zhang,[3] Jing Wen,[3] Xu-Lin Zhang,[4,5] C. T. Chan,[5] Andrea Alù,[6,7,†] Cheng-Wei Qiu,[2,‡] and Lin Chen[1,§]

[1]*Wuhan National Laboratory for Optoelectronics, Huazhong University of Science and Technology, Wuhan 430074, China*
[2]*Department of Electrical and Computer Engineering, National University of Singapore, Singapore 117583, Singapore*
[3]*Engineering Research Center of Optical Instrument and Systems, Ministry of Education and Shanghai Key Lab of Modern Optical System, University of Shanghai for Science and Technology, No. 516 Jungong Road, Shanghai 200093, China*
[4]*State Key Laboratory of Integrated Optoelectronics, College of Electronic Science and Engineering, Jilin University, Changchun 130012, China*
[5]*Department of Physics, The Hong Kong University of Science and Technology, Clear Water Bay, Hong Kong 999077, China*
[6]*Photonics Initiative, Advanced Science Research Center, City University of New York, New York, New York 10031, USA*
[7]*Physics Program, Graduate Center, City University of New York, New York, New York 10016, USA*

(Received 25 June 2020; accepted 6 October 2020; published 30 October 2020)

Dynamically encircling exceptional points (EPs) can lead to chiral mode switching as the system parameters are varied along a path that encircles EP. However, conventional encircling protocols result in low transmittance due to path-dependent losses. Here, we present a paradigm to encircle EPs that includes fast Hamiltonian variations on the parameter boundaries, termed Hamiltonian hopping, enabling ultrahigh-efficiency chiral mode switching. This protocol avoids path-dependent loss and allows us to experimentally demonstrate nearly 90% efficiency at 1550 nm in the clockwise direction, overcoming a long-standing challenge of non-Hermitian optical systems and powering up new opportunities for EP physics.

DOI: 10.1103/PhysRevLett.125.187403

Exceptional points (EPs) are degeneracies arising in non-Hermitian systems at which two or more eigenvalues and eigenstates coalesce [1]. They are at the origin of exotic phenomena that have no Hermitian counterparts, and hence have attracted significant interest in acoustics, quantum mechanics, thermodynamics, and optics. The possibility of introducing and controlling the distribution of gain and loss in photonic systems, in particular, has recently enabled the observation of EPs and their associated non-Hermitian phenomena in a wide range of optical configurations [2], including microcavities [3–6], coupled waveguides [1,7–17], gratings [18,19], and photonic crystals [20,21]. Particularly intriguing phenomena have been found when these systems are steered along a path in parameter space that encircles an EP. Owing to the topological features of complex-valued energy spectra around the EP, which form a self-intersecting Riemann surface [22], new exotic phenomena emerge, including enhanced sensing [5,6], unidirectional invisibility [18,19], topological energy transfer [23,24], chiral dynamics [9–17,25–27], effects of fundamental importance for breakthrough technology.

The topological features of EPs, such as state flip and accumulated Berry phase, can be observed in the adiabatic evolution of the system parameters around an EP in a quasidynamic approach [28,29]. The Berry phase is π when the Hamiltonian encircles EP twice, indicating that the energy spectra surface is self-intersecting around the EP. Recent work on dynamical non-Hermitian systems due to the presence of absorption has demonstrated that the evolution of states can undergo nonadiabatic transitions (NATs) due to path-dependent loss [7]. These transitions result in counterintuitive and technologically relevant chiral responses, based on which encircling an EP in the clockwise (CW) or anticlockwise (ACW) direction leads to different final states. Such a chiral response is unrealizable in a static [1] or quasistatic [28,29] Hamiltonian system, where the final state is independent of the input direction. The chiral dynamics has been experimentally demonstrated by mapping the required Hamiltonian parameters onto parity-time symmetric arrangements of waveguides in order to realize asymmetric mode switching [9,12]. However, the transmission efficiencies realized in all previous studies are very low, largely because they inherently rely on path-dependent losses arising from the slow encircling along a continuous path near the EP [9,13,14,17]. Owing to this inherently low efficiency, technological applications of chiral transmission and other non-Hermitian phenomena remain out of reach. The realization of practical non-Hermitian photonic devices and systems requires EP-encircling protocols that can realize high transmission efficiency without gain.

Here, we overcome this challenge by demonstrating an encircling protocol that takes advantage of rapid Hamiltonian variations on the parameter boundaries,

termed "Hamiltonian hopping," which enable robust chiral mode switching with near-unity efficiency. We show that the eigenstates of the system Hamiltonian converge as its parameters approach infinity, and that the chiral dynamics associated with the corresponding EP can be accessed without path-dependent loss by transitioning between these states. Chiral mode switching is theoretically predicted and experimentally demonstrated by mapping the required Hamiltonian parameters onto suitably designed coupled waveguides on standard silicon-on-insulator platform. We show that the proposed protocol can achieve in principle near-unity transmission efficiency over the entire telecommunication spectrum due to the robustness against the encircling pathway, and we experimentally demonstrate nearly 90% efficiency at 1550 nm.

For an arbitrary order Hamiltonian, the non-Hermitian dynamics as the system changes in time can be described by the evolution equation $(\partial/\partial\tau)|\psi(\tau)\rangle = iH_n(\tau)|\psi(\tau)\rangle$, where $H_n(\tau)$ is an $n \times n$ matrix, $|\psi(\tau)\rangle$ is the system state at time τ and i is the imaginary unit. For a second-order system that has two entities coupled with each other, the Hamiltonian $H_2(\tau)$ can be written as

$$H_2(\tau) = \begin{bmatrix} \beta(\tau) + i\gamma(\tau) & \kappa(\tau) \\ \kappa(\tau) & -\beta(\tau) - i\gamma(\tau) \end{bmatrix}, \quad (1)$$

where $|\psi(\tau)\rangle = [b_1(\tau), b_2(\tau)]^T$, and $\beta(\tau)$, $\gamma(\tau)$, and $\kappa(\tau)$ represent the degree of detuning, relative gain or loss rate, and coupling strength of the system, respectively. The eigenvalues are $E = \pm\sqrt{\kappa^2 + (\beta + i\gamma)^2}$ and the corresponding eigenstates $X = [\sqrt{1 \pm M}, \pm\sqrt{1 \mp M}]^T$, where $M = (\beta + i\gamma)/\sqrt{\kappa^2 + (\beta + i\gamma)^2}$, indicating that the system has an EP at $(\beta/\kappa, \gamma/\kappa) = (0, 1)$. For a general coupled system with unbalanced detuning or gain or loss rate, the coupling equations can also be transformed to the gain or loss balancing form as Eq. (1) by using a suitable gauge transformation (Supplemental Material [30], note 1). Assuming that H_2 remains constant over the time interval $[\tau_0, \tau]$, associated with the two eigenvalues and eigenstates E_1 $[\mathrm{Im}(E_1) \le 0]$, E_2 $[\mathrm{Im}(E_2) \ge 0]$, and X_1, X_2, respectively, the state evolution can be written as

$$|\psi(\tau)\rangle = c_1(\tau_0)e^{iE_1(\tau-\tau_0)}X_1 + c_2(\tau_0)e^{iE_2(\tau-\tau_0)}X_2 \quad (2)$$

if the initial state is expressed as $|\psi(\tau_0)\rangle = c_1(\tau_0)X_1 + c_2(\tau_0)X_2$, with c_1 and c_2 being arbitrary coefficients. The mathematical form of $|\psi(\tau)\rangle$ indicates that the real parts of the eigenvalues cause phase variations, while the imaginary parts lead to amplitude changes. As previously reported, the chiral dynamics in a lossy non-Hermitian system relies on slowly encircling the EP with path-dependent loss [1,9–17,34], which leads to very low transmittance for the output state [9,13,14,17].

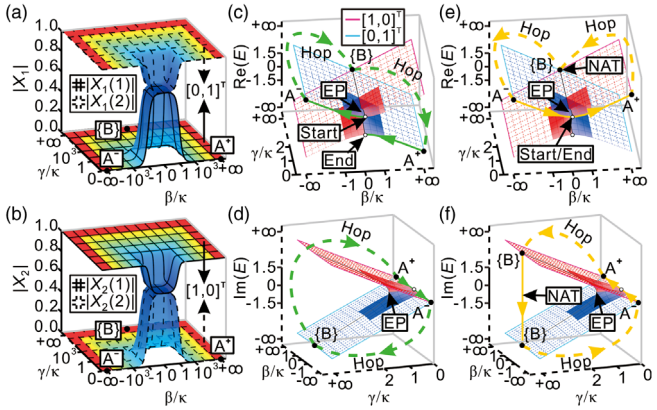

FIG. 1. (a),(b) Amplitudes of $X_1 = [X_1(1), X_1(2)]^T$ and $X_2 = [X_2(1), X_2(2)]^T$ of H_2 in the parameter space described by β/κ and γ/κ. The surfaces covered by solid and dashed meshes represent the amplitudes of the first and second terms of X_1 (a) [X_2 (b)], respectively. Red regions represent the parameter space boundaries that share the same convergent eigenstates as $[0, 1]^T$ and $[1, 0]^T$. (c),(d) CW and (e),(f) ACW Hamiltonian-hopping-assisted loop around EP in the Riemann surfaces formed by the real part $\mathrm{Re}(E)$ and imaginary part $\mathrm{Im}(E)$ of the energy spectra of H_2. The red and blue surfaces denote $\mathrm{Im}(E) \ge 0$ and $\mathrm{Im}(E) \le 0$, respectively. The surfaces formed by the dotted lines symbolically show β/κ or γ/κ extending to infinity. The two eigenvalues, associated with $[1, 0]^T$ and $[0, 1]^T$, are denoted by magenta and cyan lines, respectively. The dashed lines indicate the Hamiltonian hopping among A^+, A^-, and $\{B\}$.

We show here how the efficiency limitation can be overcome by encircling an EP with Hamiltonian hopping on the parameter boundaries. Figures 1(a) and 1(b) show the amplitudes of X_1 and X_2 in the parameter space of H_2 as a function of β/κ and γ/κ (>0). The corresponding phase can be found in Fig. S1 of the Supplemental Material [30]. When H_2 approaches the parameter space boundaries ($\beta/\kappa \to \pm\infty$ and/or $\gamma/\kappa \to +\infty$), the two eigenstates converge to $X_1 = [0, 1]^T$ and $X_2 = [1, 0]^T$. When H_2 is far from the parameter space boundaries, we have two distinct eigenstates. Consider two points $[A^+ : (\beta/\kappa, \gamma/\kappa) \to (+\infty, 0)$ and $A^- : (\beta/\kappa, \gamma/\kappa) \to (-\infty, 0)]$ and a point set $\{B\} : (\beta/\kappa, \gamma/\kappa) \to (R, +\infty)$ on the parameter space boundaries, where R denotes an arbitrary real value. The system state $(c_1[0, 1]^T + c_2[1, 0]^T)$ will have the same coefficients c_1 and c_2 when the Hamiltonian hops between $A^+(A^-)$ and $\{B\}$ (see the Supplemental Material [30], note 3). It is worth stressing that, the eigenstate $[1, 0]^T$ at $\{B\}$, associated with the imaginary part of the eigenvalue, $+\infty i$, suffers from very large loss. On the contrary, the other eigenstate $[0, 1]^T$ at $\{B\}$ has the imaginary part of the eigenvalue, $-\infty i$, and for a purely lossy system, the eigenvalue of $[0, 1]^T$ at $\{B\}$ has the imaginary part of zero as $-i\gamma$ is removed in Eq. (1), hence it is lossless due to the significant coupling mismatch.

The approach of using Hamiltonian hopping along the parameter space boundaries mentioned above inspires us to build a Hamiltonian-hopping-assisted loop around an EP that does not suffer from path-dependent loss. Figures 1(c)–1(f) show the dynamic trajectory of the second-order Hamiltonian for CW [Figs. 1(c) and 1(d)] and ACW [Figs. 1(e) and 1(f)] Hamiltonian-hopping-assisted loop around the EP. For a CW loop, the Hamiltonian starts at the origin, $(\beta/\kappa, \gamma/\kappa) = (0, 0)$, associated with the initial eigenstate of $|\psi(\tau_0)\rangle = [1, 1]^T$ (the other eigenstate is $[1, -1]^T$). Next, $H_2(\tau)$ evolves slowly along the edge ($\gamma = 0$) of the Riemann surface, and reaches A^- at τ_{B1}. Because of the adiabatic theorem, the state at A^- can be expressed as $|\psi(\tau_{B1})\rangle = X_1(\tau_{B1}) + \varepsilon X_2(\tau_{B1})$, where $X_1(\tau_{B1}) = [0, 1]^T$, $X_2(\tau_{B1}) = [1, 0]^T$, and ε is a small number, originating from the fact that $\partial H_2(\tau)/\partial\tau \to 0$ is not strictly fulfilled. Next, $H_2(\tau)$ hops from A^- to $\{B\}$ at τ_{B1}, and stays there for a time interval $[\tau_{B1}, \tau_{B2}]$. According to Eq. (2), the state at τ_{B2} is $|\psi(\tau_{B2})\rangle = \exp(i\int_{\tau_{B1}}^{\tau_{B2}} E_1^B\, d\tau)X_1(\tau_{B1}) + \varepsilon \exp(i\int_{\tau_{B1}}^{\tau_{B2}} E_2^B\, d\tau)X_2(\tau_{B1})$, where E_1^B $[\mathrm{Im}(E_1^B) \to -\infty]$ and E_2^B $[\mathrm{Im}(E_2^B) \to +\infty]$ are the two eigenvalues of $H_2(\tau)$ at $\{B\}$. Thus, the ratio $X_1(\tau_{B1})/X_2(\tau_{B1})$ increases as time progresses, and reaches its maximum value at τ_{B2}. $H_2(\tau)$ then hops to A^+ at τ_{B2}, and then evolves slowly along the edge ($\gamma = 0$) to return to the starting position at τ_{end}. The final state can be expressed as $|\psi(\tau_{\mathrm{end}})\rangle = X_1(\tau_{\mathrm{end}}) + \varepsilon X_2(\tau_{\mathrm{end}})$ with $X_1(\tau_{\mathrm{end}}) = [1, -1]^T$ and $X_2(\tau_{\mathrm{end}}) = [1, 1]^T$, and is further simplified as $|\psi(\tau_{\mathrm{end}})\rangle = [1, -1]^T$ by neglecting ε. The convergent eigenstate $[0, 1]^T$, denoted by cyan lines on the parameter space boundaries in Fig. 1(c), is always the dominant eigenstate at A^+, A^-, and $\{B\}$ for the CW loop. The self-intersecting Riemann surface features sustained by the EP make sure that $[0, 1]^T$ lies on the upper Riemann surface at A^- and on the lower Riemann surface at A^+, hence the initial state $[1, 1]^T$ on the upper surface switches to the final state $[1, -1]^T$ on the lower surface.

Let us now consider the reverse ACW loop. Initially, $H_2(\tau)$ evolves to $H_2(\tau_{B2})$ at A^+, associated with $|\psi(\tau_{B2})\rangle = [1, 0]^T + \varepsilon[0, 1]^T$, and hops to $\{B\}$. The state can be described as $|\psi(\tau_{B1})\rangle = \exp(i\int_{\tau_{B1}}^{\tau_{B2}} E_2^B d\tau)[1, 0]^T + \varepsilon \exp(i\int_{\tau_{B1}}^{\tau_{B2}} E_1^B d\tau)[0, 1]^T$ at τ_{B1}, with the ratio $[0, 1]^T/[1, 0]^T$ being much larger than 1 under the condition $\mathrm{Im}(E_1^B) \to -\infty$ and $\mathrm{Im}(E_2^B) \to +\infty$. In other words, a NAT occurs and the state can be further simplified as $|\psi(\tau_{B1})\rangle = [0, 1]^T + \varepsilon[1, 0]^T$ at τ_{B1}. Finally, $H_2(\tau)$ hops from $\{B\}$ to A^- and slowly evolves into the starting position with the final state of $|\psi(\tau_0)\rangle = [1, 1]^T$. In the aforementioned analysis, the hopping time is neglected since the Hamiltonian hopping takes a very short time. It can be proven, however, that a chiral response can also be observed if the Hamiltonian hopping takes a long time (Supplemental Material [30], Note 4). It is also worth emphasizing here that the final state is always $[1, -1]^T$ for CW loop and $[1, 1]^T$ for ACW loop, no matter which eigenstate is chosen as the starting state (Supplemental Material [30], note 5).

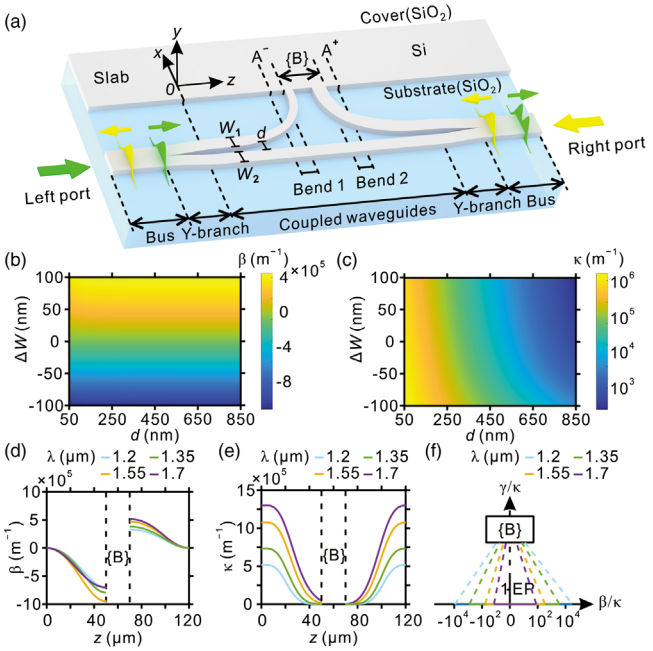

FIG. 2. (a) Double-coupled silicon waveguides for state evolution in a Hamiltonian-hopping-assisted loop around EP. The width of the first (second) waveguide is W_1 (W_2) and d is the separation distance between the two waveguides. (b),(c) β and κ as a function of ΔW and d at 1550 nm. (d),(e) Retrieved β and κ along the z direction in the region of the coupled waveguides. (f) Hamiltonian-hopping-assisted loop around EP for different wavelengths.

The system does not suffer from dissipation as the state moves along the edge of the Riemann surface ($\gamma = 0$). For the CW process, the triggered eigenstate X_2 $[\mathrm{Im}(E_2) \geq 0]$, which takes up a small portion of the system energy, is dissipated in the time interval (τ_{B1}, τ_{B2}) so that almost no energy is lost in the entire process. For the ACW process, loss merely arises during the NAT process in the time interval (τ_{B2}, τ_{B1}). Hence, compared with the previous path-dependent loops in purely lossy systems [9,13,14,17], the proposed Hamiltonian-hopping-assisted loop is capable of highly suppressing energy dissipation (Supplemental Material [30], note 6). The chiral dynamics around the EP with this Hamiltonian-hopping-assisted loop takes advantage of the EP topological features, but avoids the insurgence of loss except for the NAT process. In addition, the low-loss chiral mode switching is robust against the specific pathway choice (Supplemental Material [30], note 7).

The required Hamiltonian parameters for Hamiltonian-hopping-assisted loop around EP can be mapped onto suitably designed purely lossy silicon coupled waveguides, schematically shown in Fig. 2(a), where the detailed structural parameters can be found in Fig. S9 of the Supplemental Material [30]. $b_1(\tau)$ and $b_2(\tau)$ are related to the complex amplitudes of the electric field in the first

and second waveguides, respectively. The eigenstates $[1,1]^T$ and $[1,-1]^T$ denote even and odd modes, respectively, associated with TE_0 and TE_1 modes in the bus waveguide. τ is mapped onto the propagation distance z. The width difference $\Delta W = W_1 - W_2$ and separation distance d between the two waveguides are mapped onto β and κ based on coupled mode theory [31]. β and κ versus ΔW and d are shown in Figs. 2(b) and 2(c) at 1550 nm (see more data at 1200 and 1700 nm in the Supplemental Material [30], Fig. S10). Figures 2(d) and 2(e) present the dependence of β and κ on z, respectively, for different wavelengths. A^+ (A^-) can be reached by increasing d, which effectively makes $\kappa \to 0$, and by adjusting ΔW to make β take a positive (negative) value. Large loss rate, γ, at $\{B\}$ can be implemented using a semi-infinite slab waveguide to replace the first waveguide. Bend waveguides are used to connect the first waveguide with the slab waveguide. Once the guided waves reach the slab waveguide through the bend, light is not reflected back, i.e., $\gamma/\kappa \to +\infty$ as required at $\{B\}$. Light input into the bus waveguides from the left (right) port indicates that the Hamiltonian evolves in the CW (ACW) direction. Figure 2(f) presents the parameter loop for the coupled waveguides at different wavelengths.

The chiral mode switching is clearly demonstrated when the TE_0 mode inputs from the left and right ports at 1550 nm [Figs. 3(a) and 3(b)], i.e., the TE_1 and TE_0 modes output from the right and left ports, respectively. For the CW direction, the TE modes are mainly distributed in the second waveguide at A^-, $\{B\}$, and A^+, consistent with the above conclusion that $[1,0]^T$ is always infinitesimal during evolution. For the ACW direction, the TE mode is mainly distributed in the first waveguide with $|\psi(\tau_{B2})\rangle \approx [1,0]^T$ at A^+. The state shifts to $[0,1]^T$ at A^- after the system undergoes NAT at $\{B\}$, associated with the electric field being located at the second waveguide.

A scanning electron microscope (SEM) image for one fabricated sample of the double-coupled silicon waveguides is shown in Fig. 3(c), and grating couplers and mode (de)multiplexers [35] are used to couple and measure TE modes (see note 8 of the Supplemental Material and Fig. S11 [30]). T_{mn} (T'_{mn}) represents the transmission efficiency of the TE_m mode from the output port as TE_n mode inputs from the left (right) port. For the left-port input, the transmission efficiency of TE_1 mode from the right port is -0.20 to -0.01 dB within 1200–1700 nm in the simulations [Fig. 3(d)], and -2.73 to -0.34 dB within 1525–1575 nm in the experiment [Fig. 3(e)]. The measurable bandwidth is limited by the operation wavelength range of the laser. The measured T_{10}, T_{00}, T'_{00}, and T'_{10} are -0.56, -14.1, -12.74, and -34.04 dB at 1550 nm, respectively, associated with mode purities of 96% and 99% for the TE_1 and TE_0 modes that output from the right and left ports, respectively. Here the mode purity is defined as the energy ratio of the desired mode to total output [36].

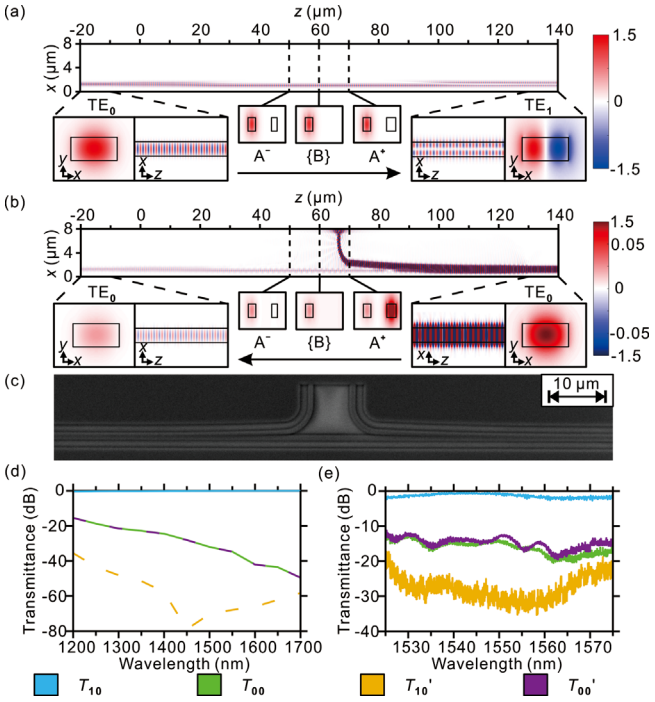

FIG. 3. (a),(b) Simulated field distributions of the transverse components of electric field (E_x) at 1550 nm. The TE_0 mode inputs from the left port (a) and right port (b), respectively. (c) SEM image of the device. (d) Simulated transmittance spectra for TE_0 and TE_1 mode at the output port over 1200–1700 nm wavelength range. Solid (dashed) lines represent input from the left (right) port. (e) Measured transmittance spectra over 1525–1575 nm wavelength range. Numerical simulations are conducted by finite-difference time domain with commercial software Lumerical FDTD Solutions.

The experimental results show some deviation from simulations, originating from fabrication error in terms of etching roughness and precision [35,37]. In light of Lorentz reciprocity theorem [38], T_{00} should be identical to T'_{00}, which is verified in simulations, but the experimental results show some minor deviation due to measurement errors probably associated to the grating couplers and noise arising from light source and spectrometer. If we take steps to increase T'_{00}, the TE_0 mode that outputs from the right port undergoes a transmission increase as well, and hence increases mode crosstalk (Supplemental Material [30], Fig. S12).

Our encircling protocol can be extended to implement a Hamiltonian-hopping-assisted loop in a higher-order Hamiltonian system. We have taken three coupled silicon waveguides as an example to build a Hamiltonian-hopping-assisted loop in a three-order Hamiltonian system (Supplemental Material [30], notes 9,10). The device is designed to output TE_2 mode for the left-port TE_0 mode input [CW direction, Fig. 4(a)], while TE_0 mode outputs for the right-port TE_0 mode input [ACW direction, Fig. 4(b)] due to the emergence of NAT. The modal field distributions at A^-, $\{B\}$, and A^+ clearly exhibit how the state evolves

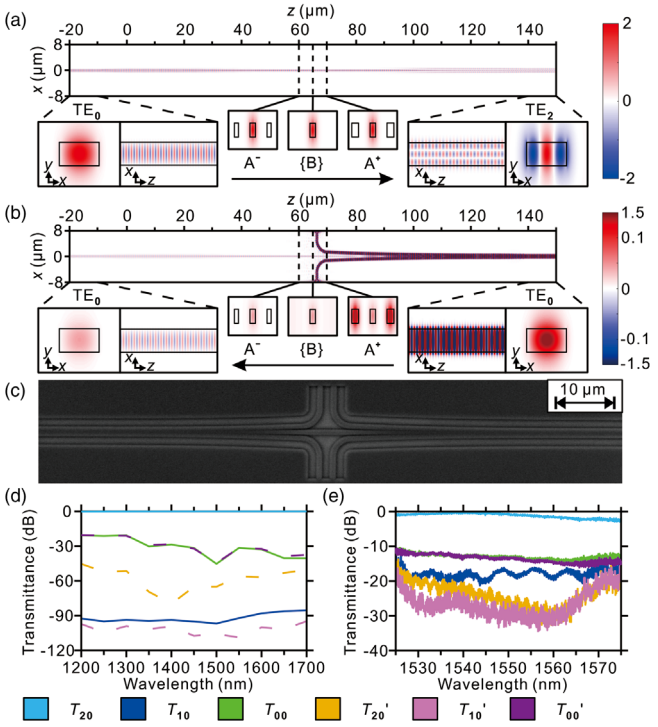

FIG. 4. (a),(b) Simulated field distributions of the transverse components of electric field (E_x) at 1550 nm. (c) SEM image of the device. (d) Simulated transmittance spectra for TE_0, TE_1, and TE_2 mode at the output port over 1200–1700 nm wavelength range. (e) Measured transmittance spectra over 1525–1575 nm wavelength range.

after the Hamiltonian hopping. The SEM image of the coupled waveguides is illustrated in Fig. 4(c). Simulated and experimental results reveal high transmission efficiencies and mode purities for the output modes over a wide spectral band [Figs. 4(d) and 4(e)]. The transmittance and mode purity are 89% (5%) and 93% (92%) for the TE_2 (TE_0) output mode at 1550 nm in the experiment, respectively. More information for demonstrating chiral dynamics with four- and five-coupled silicon waveguides can be found in Figs. S16 and S17 of the Supplemental Material [30].

In conclusion, we have introduced the concept of Hamiltonian hopping and demonstrated low-loss and robust chiral mode switching via rapid Hamiltonian transitions between convergent eigenstates in EP encircling. This protocol exploits the convergence of the system eigenstates as its Hamiltonian parameters approach infinity, and it overcomes path-dependent losses that have limited the achievable transmission efficiency in previous demonstrations of EP encircling. Counterintuitively, near-unity efficiency of chiral transmission results from the addition of large loss rate in the optical system. These results enable non-Hermitian dynamics to be efficiently harnessed not only in optics, but also acoustics, electronics, and condensed matter physics, for practical devices and applications based on exceptional-point physics.

This project is supported by the National Major Research and Development Program (No. 2018YFB2200200, No. 2018YFB2201901), National Natural Science Foundation of China (11674118, 12074137), State Key Laboratory of Advanced Technology for Materials Synthesis and Processing (Wuhan University of Technology), RGC Hong Kong (16303119, AoE/P-02/12). A. A. acknowledges support from the Air Force Office of Scientific Research, the Simons Foundation and the National Science Foundation. C. W. Q. acknowledges the support from the National Research Foundation, Prime Minister's Office, Singapore under its Competitive Research Program (CRP award NRF CRP22-2019-0006).

*These authors contributed equally to this work.
†Corresponding author.
aalu@gc.cuny.edu
‡Corresponding author.
chengwei.qiu@nus.edu.sg
§Corresponding author.
chen.lin@mail.hust.edu.cn

[1] A. Guo, G. J. Salamo, D. Duchesne, R. Morandotti, M. Volatier-Ravat, V. Aimez, G. A. Siviloglou, and D. N. Christodoulides, Observation of PT-Symmetry Breaking in Complex Optical Potentials, Phys. Rev. Lett. **103**, 093902 (2009).
[2] M.-A. Miri and A. Alù, Exceptional points in optics and photonics, Science **363**, eaar7709 (2019).
[3] L. Feng, Z. J. Wong, R.-M. Ma, Y. Wang, and X. Zhang, Single-mode laser by parity-time symmetry breaking, Science **346**, 972 (2014).
[4] B. Peng, Ş. K. Özdemir, F. Lei, F. Monifi, M. Gianfreda, G. Lu Long, S. Fan, F. Nori, C. M. Bender, and L. Yang, Parity–time-symmetric whispering-gallery microcavities, Nat. Phys. **10**, 394 (2014).
[5] H. Hodaei, A. U. Hassan, S. Wittek, H. Garcia-Gracia, R. El-Ganainy, D. N. Christodoulides, and M. Khajavikhan, Enhanced sensitivity at higher-order exceptional points, Nature (London) **548**, 187 (2017).
[6] W. Chen, Ş. Kaya Özdemir, G. Zhao, J. Wiersig, and L. Yang, Exceptional points enhance sensing in an optical microcavity, Nature (London) **548**, 192 (2017).
[7] E.-M. Graefe, A. A. Mailybaev, and N. Moiseyev, Breakdown of adiabatic transfer of light in waveguides in the presence of absorption, Phys. Rev. A **88**, 033842 (2013).
[8] S. Ke, B. Wang, C. Qin, H. Long, K. Wang, and P. Lu, Exceptional points, and asymmetric mode switching in plasmonic waveguides, J. Lightwave Technol. **34**, 5258 (2016).
[9] J. Doppler, A. A. Mailybaev, J. Böhm, U. Kuhl, A. Girschik, F. Libisch, T. J. Milburn, P. Rabl, N. Moiseyev, and S. Rotter, Dynamically encircling an exceptional point for asymmetric mode switching, Nature (London) **537**, 76 (2016).
[10] S. N. Ghosh and Y. D. Chong, Exceptional points and asymmetric mode conversion in quasi-guided dual-mode optical waveguides, Sci. Rep. **6**, 19837 (2016).

[11] A. U. Hassan, B. Zhen, M. Soljačić, M. Khajavikhan, and D. N. Christodoulides, Dynamically Encircling Exceptional Points: Exact Evolution and Polarization State Conversion, Phys. Rev. Lett. **118**, 093002 (2017).
[12] J. W. Yoon, Y. Choi, C. Hahn, G. Kim, S. Ho Song, K.-Y. Yang, J. Yub Lee, Y. Kim, C. S. Lee, J. K. Shin, H.-S. Lee, and P. Berini, Time-asymmetric loop around an exceptional point over the full optical communications band, Nature (London) **562**, 86 (2018).
[13] X.-L. Zhang, S. Wang, B. Hou, and C. T. Chan, Dynamically Encircling Exceptional Points: In situ Control of Encircling Loops and the Role of the Starting Point, Phys. Rev. X **8**, 021066 (2018).
[14] X.-L. Zhang, T. Jiang, and C. T. Chan, Dynamically encircling an exceptional point in anti-parity-time symmetric systems: asymmetric mode switching for symmetry-broken modes, Light Sci. Appl. **8**, 88 (2019).
[15] X.-L. Zhang and C. T. Chan, Dynamically encircling exceptional points in a three-mode waveguide system, Commun. Phys. **2**, 63 (2019).
[16] X.-L. Zhang, J.-F. Song, C. T. Chan, and H.-B. Sun, Distinct outcomes by dynamically encircling an exceptional point along homotopic loops, Phys. Rev. A **99**, 063831 (2019).
[17] Q. Liu, S. Li, B. Wang, S. Ke, C. Qin, K. Wang, W. Liu, D. Gao, P. Berini, and P. Lu, Efficient Mode Transfer on a Compact Silicon Chip by Encircling Moving Exceptional Points, Phys. Rev. Lett. **124**, 153903 (2020).
[18] Z. Lin, H. Ramezani, T. Eichelkraut, T. Kottos, H. Cao, and D. N. Christodoulides, Unidirectional Invisibility Induced by PT-Symmetric Periodic Structures, Phys. Rev. Lett. **106**, 213901 (2011).
[19] L. Feng, Y.-L. Xu, W. S. Fegadolli, M.-H. Lu, J. E. B. Oliveira, V. R. Almeida, Y.-F. Chen, and A. Scherer, Experimental demonstration of a unidirectional reflectionless parity-time metamaterial at optical frequencies, Nat. Mater. **12**, 108 (2013).
[20] H. Zhou, J. Y. Lee, S. Liu, and B. Zhen, Exceptional surfaces in PT-symmetric non-Hermitian photonic systems, Optica **6**, 190 (2019).
[21] X.-X. Li, S.-f. Ye, L.-X. Yang, and Y.-T. Fang, Asymmetric and dynamic waveguide propagation based on localized parity-time symmetry, Opt. Commun. **443**, 129 (2019).
[22] W. D. Heiss, Repulsion of resonance states and exceptional points, Phys. Rev. E **61**, 929 (2000).
[23] C. Dembowski, H.-D. Gräf, H. L. Harney, A. Heine, W. D. Heiss, H. Rehfeld, and A. Richter, Experimental Observation of the Topological Structure of Exceptional Points, Phys. Rev. Lett. **86**, 787 (2001).
[24] H. Xu, D. Mason, L. Jiang, and J. G. E. Harris, Topological energy transfer in an optomechanical system with exceptional points, Nature (London) **537**, 80 (2016).
[25] M. Berry and R. Uzdin, Slow non-Hermitian cycling: exact solutions and the Stokes phenomenon, J. Phys. A **44**, 435303 (2011).
[26] R. Uzdin, A. Mailybaev, and N. Moiseyev, On the observability and asymmetry of adiabatic state flips generated by exceptional points, J. Phys. A **44**, 435302 (2011).
[27] T. J. Milburn, J. Doppler, C. A. Holmes, S. Portolan, S. Rotter, and P. Rabl, General description of quasiadiabatic dynamical phenomena near exceptional points, Phys. Rev. A **92**, 052124 (2015).
[28] C. Dembowski, B. Dietz, H.-D. Gräf, H. L. Harney, A. Heine, W. D. Heiss, and A. Richter, Encircling an exceptional point, Phys. Rev. E **69**, 056216 (2004).
[29] T. Gao, E. Estrecho, K. Y. Bliokh, T. C. H. Liew, M. D. Fraser, S. Brodbeck, M. Kamp, C. Schneider, S. Höfling, Y. Yamamoto, F. Nori, Y. S. Kivshar, A. G. Truscott, R. G. Dall, and E. A. Ostrovskaya, Observation of non-Hermitian degeneracies in a chaotic exciton-polariton billiard, Nature (London) **526**, 554 (2015).
[30] See Supplemental Material at http://link.aps.org/supplemental/10.1103/PhysRevLett.125.187403 for more details on coupled mode equations, phase of the two eigenstates, the eigenstate coefficients after Hamiltonian hopping, dynamics of Hamiltonian-hopping-assisted loops, comparison for different loops, the structural parameters, experimental setup, measurement results, and Hamiltonian-hopping-assisted loop for high-order system, which includes Refs. [12,31–33].
[31] C. Shun-Lien, A coupled mode formulation by reciprocity and a variational principle, J. Lightwave Technol. **5**, 5 (1987).
[32] B. N. Parlett, *The Symmetric Eigenvalue Problem* (Prentice Hall, Englewood Cliffs, NJ, 1980).
[33] S. Noschese, L. Pasquini, and L. Reichel, Tridiagonal Toeplitz matrices: properties and novel applications. Numer. Linear Algebra Appl. **20**, 302 (2013).
[34] A. U. Hassan, G. L. Galmiche, G. Harari, P. LiKamWa, M. Khajavikhan, M. Segev, and D. N. Christodoulides, Chiral state conversion without encircling an exceptional point, Phys. Rev. A **96**, 052129 (2017).
[35] D. Dai, C. Li, S. Wang, H. Wu, Y. Shi, Z. Wu, S. Gao, T. Dai, H. Yu, and H.-K. Tsang, 10-channel mode (de)multiplexer with dual polarizations, Laser Photonics Rev. **12**, 1700109 (2018).
[36] Z. Li, M.-H. Kim, C. Wang, Z. Han, S. Shrestha, A. C. Overvig, M. Lu, A. Stein, A. M. Agarwal, M. Lončar, and N. Yu, Controlling propagation, and coupling of waveguide modes using phase-gradient metasurfaces, Nat. Nanotechnol. **12**, 675 (2017).
[37] S. Li, Y. Zhou, J. Dong, X. Zhang, E. Cassan, J. Hou, C. Yang, S. Chen, D. Gao, and H. Chen, Universal multimode waveguide crossing based on transformation optics, Optica **5**, 1549 (2018).
[38] R. J. Potton, Reciprocity in optics, Rep. Prog. Phys. **67**, 717 (2004).